



OPEN ACCESS

EDITED BY

Fengmei Jing,
Beijing Institute of Technology, China

REVIEWED BY

Yang Luo,
Northwestern Polytechnical University, China
Yang Zhou,
University of Strathclyde, United Kingdom

*CORRESPONDENCE

Mingxin Li,
✉ mingxin.li@just.edu.cn

RECEIVED 10 January 2024

ACCEPTED 04 March 2024

PUBLISHED 13 March 2024

CITATION

Yuan H, Chen Y, Li M, Chen L, Bai X and Li Y (2024), Scale-sensitivity analysis for floating energy production system with anti-motion structure under high sea conditions. *Front. Energy Res.* 12:1368327. doi: 10.3389/fenrg.2024.1368327

COPYRIGHT

© 2024 Yuan, Chen, Li, Chen, Bai and Li. This is an open-access article distributed under the terms of the [Creative Commons Attribution License \(CC BY\)](https://creativecommons.org/licenses/by/4.0/). The use, distribution or reproduction in other forums is permitted, provided the original author(s) and the copyright owner(s) are credited and that the original publication in this journal is cited, in accordance with accepted academic practice. No use, distribution or reproduction is permitted which does not comply with these terms.

Scale-sensitivity analysis for floating energy production system with anti-motion structure under high sea conditions

Hongtao Yuan^{1,2}, Yi Chen³, Mingxin Li^{3*}, Linfeng Chen³, Xu Bai³ and Yongzheng Li³

¹College of Naval Engineering, Harbin Engineering University, Harbin, China, ²Shanghai Waigaoqiao Shipbuilding and Ocean Engineering Co., LTD., Shanghai, China, ³School of Naval Architecture and Ocean Engineering, Jiangsu University of Science and Technology, Zhenjiang, China

The heave motion of a new cylindrical floating drilling production storage and offloading system (FDPSO) with extended cylinder, anti-motion structure and a gap between the extended cylinder and anti-motion structure under high sea conditions was investigated by implementing numerical simulations for its reduced-scale laminar flow model (1:77.8) using the CFD software STAR-CCM+. The effect of changing the width (10 ~ 15 m) and height (10 ~ 15 m) of the anti-motion structure on the heave motion of the new cylindrical FDPSO were analyzed. The results show that increasing the width and height of the anti-motion structure increases the natural period of the structural heave motion, making it far away from the main energy period of the wave, and has a certain inhibitory effect on the heave motion of the FDPSO. Comparing the variation of vortex field around the structures of different sizes, it is concluded that the vortex generation and vortex shedding around the highwidth anti-motion structure model is significantly strengthened compared with the low-width anti-motion structure model. The variation of the vortex generation and vortex shedding due to the change in height is relatively inferior compared to the change in width.

KEYWORDS

cylindrical FDPSO, anti-motion structure, heave motion, CFD, scale sensitivity

1 Introduction

“Floating Drilling Production Storage and Offloading System (FDPSO)” refers to adding drilling functions to an FPSO. It is a floating container-shaped production system that integrates offshore oil and gas processing, oil storage and offloading, power generation, heating, control, and living functions. FDPSO has many advantages, including low initial investment, short construction period, strong oil storage capacity, adaptable to a wide range of water depths, easy to relocate, and reusable. It is widely used in deep-sea, shallow-sea, and marginal oil fields. Most of the offshore oil and gas fields being developed or about to be developed in China belong to the category of marginal oil fields (Wang and Feng, 2011). The constant wear and corrosion of infrastructure in harsh underwater environments drives up maintenance costs, and these tasks are currently carried out primarily with remotely operated vehicles (ROVs), which often require tethered and human operators, or with autonomous underwater vehicles (AUVs), which are

limited in their accessibility and maneuverability. In order to reduce the risk and cost of manual maintenance, underwater bionic robots can be used to check and measure underwater cables, offshore wind farms, electric fields and other underwater infrastructure (Gorma et al., 2021). Therefore, FDPPO is quite suitable for the development of China's offshore oil and gas fields. After long-term development, a variety of new forms of FDPPO have emerged, including deepwater octagonal FDPPO, hourglass-shaped FDPPO, multicylinder FDPPO, and cylindrical FDPPO. Through motion response analysis of cylindrical FDPPO, it is found that cylindrical FDPPO has advantages such as low investment, low cost, and short construction period, but also has some drawbacks, such as large sway motion amplitude.

A motion response analysis of the cylindrical FDPPO reveals both strengths and weaknesses, with significant heave motion amplitudes as a drawback. To develop an internationally advanced FDPPO, Wang Shisheng (Wang and Zhao, 2014) and others conducted a conceptual design study on the deepwater octagonal FDPPO. They analyzed the impact of different oscillation plate sizes on the inherent characteristics of the octagonal FDPPO and the influence of different floating body diameters on the motion performance. Results indicate that increasing the oscillation plate size significantly alters the inherent period of the floating body. Addressing the poor wave resistance of ship-shaped FPSO, Zhao Zhijuan (Zhao, 2012) innovatively designed a new multi-cylinder FDPPO suitable for operations in the South China Sea. Computational analysis demonstrates that the inherent period of the multi-cylinder FDPPO can stay away from its wave period. Yao Yuxin (Yao and Wang, 2015) proposed a novel hourglass-shaped floating production storage and offloading system, analyzing the effects of oscillatory motion response, viscous damping, and nonlinear stiffness on the heave motion performance of the hourglass-shaped floater. This provides guidelines for the outer shape design of new floating production units. Liu Liqin (Liu and Zhang, 2019), following the SEVEN-type FPSO's outer shape, modified the oscillation plate structure by removing the slope foot connecting the cylinder and oscillation plate, adding inclined oscillation plates. The study investigates the impact of different sea conditions on the inclination angle of the oscillation plate on its damping characteristics and anti-rolling effects. Research findings indicate that smaller cone angles provide better suppression of structural heave motion, with a 10° cone angle performing well in inhibiting longitudinal sway under various sea conditions. Ji et al., 2022 found a new drive line immersion boundary mixing method for predicting the wake characteristics of horizontal axis wind turbines. Zeng et al., 2024 summarized the research progress of nonlinear fluid dynamics of floating offshore wind turbines. Zeng et al., 2023 studied the high order harmonic load and low frequency resonance response of offshore floating wind turbine under extreme wave group. Zeng et al., 2021 conducted numerical and experimental studies on the wave breaking power of a single pile offshore wind turbine. Li et al., 2023a conducted a numerical simulation of scour waves generated by ship movement over an uneven seafloor. Li et al., 2023b studied the waves produced when a ship passes through a change in depth. Li et al., 2023c studied the interference effect of upstream waves generated by depth changes in catamarans. Li et al., 2023d conducted a time domain numerical simulation of positive speed motion of multiple ships in waves. Li et al., 2019 studied stable hydrodynamic interactions between human swimmers.

This paper conducts CFD (Computational Fluid Dynamics) numerical simulation analysis on the heave motion of a cylindrical

FDPPO equipped with extended cylindrical bodies and a box-type motion reduction structure. Various height and width conditions of the motion reduction structure are considered to investigate their impact on the heave motion of the cylindrical FDPPO. The numerical simulation provides heave motion and vertical force time history curves, enabling an analysis of the influence of the motion reduction structure's width and height. Additionally, the study elucidates the physical mechanisms behind how the dimensions of the motion reduction structure affect the heave motion of the FDPPO, based on the flow field information obtained from numerical simulations.

2 Mathematical models and numerical methods

2.1 Governing equations for incompressible viscous fluids

In the numerical simulation of this paper, the hydrodynamic load of the floating drilling production storage and unloading device is obtained by solving the incompressible viscous fluid outside the device. In three dimensions, for a homogeneous incompressible fluid, the density of the fluid remains constant during the motion, then the N-S equations for the three-dimensional incompressible viscous fluid can be expressed as:

$$\operatorname{div} v = 0 \quad (1)$$

$$\rho Dv/Dt = \rho F_b - \operatorname{grad} p + \mu \nabla^2 v \quad (2)$$

where: v is the fluid velocity vector; p is the pressure per unit volume of fluid; F_b is the mass force per unit volume; ρ is fluid density; μ is the viscosity coefficient of the fluid. ρ and μ are calculated according to the free surface capture method.

2.2 Free surface capture method

In this paper, the numerical simulation involves the study of water and air two-phase flow. Euler-Euler model is used to describe the two-phase fluid in the calculation domain, and the VOF (Hirt and Nichols, 1981) (Volume of Fluid) method and the variable of phase volume fraction is introduced to track the phase interface in the calculation domain (Guo, 2017).

The fractional function of the VOF model is:

$$\begin{cases} \alpha = 0 & \text{air} \\ 0 < \alpha < 1 & \text{interface} \\ \alpha = 1 & \text{water} \end{cases} \quad (3)$$

The transport equation of the VOF model function follows the convection equation as follows:

$$\frac{\partial \alpha}{\partial t} + \nabla \cdot (\mathbf{U}\alpha) + \nabla \cdot (\mathbf{U}_r(1 - \alpha)\alpha) = 0 \quad (4)$$

where \mathbf{U} is the fluid velocity and \mathbf{U}_r is the velocity field used to compress the interface.

The density and viscosity in the continuity equation and momentum equation above are obtained by weighted average of the proportion of the two-phase fluid, and the function is as follows:

TABLE 1 Wave parameters.

Sea state parameter	Actual sea state	Sea state after scale
Wave spectrum	JONSWAP	JONSWAP
Wind speed/m·s ⁻¹	57.2	6.48
Significant wave height/m	12.7	0.16
Spectral peak period/s	15	1.7
Surface flow rate/m·s ⁻¹	2.49	0.28
Wind, wave and current in the same direction/(°)	0	0

TABLE 2 Physical parameters.

Platform parameter	Actual FDPSO dimensions	Scale FDPSO size
Scale ratio	1:77.8	
Cylinder diameter/m	76	0.9768
Reduced structure height/m	10	0.1285
External diameter of reduced structure/m	98	1.2600
Extended cylinder height/m	15	0.1928
Depth of barrel body/m	35	0.4500
Draft/m	40	0.5141
Reduced structural clearance/m	1	0.0129
Lunar pool diameter/m	apex	12
	Extremitas inferior	18

$$\rho = \alpha\rho_w + (1 - \alpha)\rho_a \tag{5}$$

$$\mu = \alpha\mu_w + (1 - \alpha)\mu_a \tag{6}$$

where subscript *w* represents water and subscript *a* represents air.

2.3 Wave generation and wave parameter setting

JONSWAP was measured and analyzed by the North Sea Wave Joint Project. The spectrum describes irregular waves (Du, 2021). The setting of wave parameters is shown in Table 1.

2.4 FDPSO motion theory

In the study of CFD numerical simulation, it is very important to solve the motion of floating body in fluid. In the case that only the single freedom motion of the floating body is considered, the motion equation of FDPSO can be established based on the direct equilibrium method of D'Alembert's principle:

$$m\ddot{y} + c\dot{y} + ky = F \tag{7}$$

Where: *m* is the mass of the floating body; *y* is the displacement of the floating body in the direction of motion; *c* is the viscous

damping coefficient; *k* is the stiffness coefficient; *F* is the exciting force on the floating body in the direction of motion.

When FDPSO does heave motion, the force *F* consists of the hydrodynamic force *F_v* and the additional mass inertial force *F_a* caused by the heave additional mass, i. e:

$$F = F_v + F_a \tag{8}$$

$$F_a = -m_a\ddot{y} \tag{9}$$

By substituting equations (8) and (9) into Equation 7, the equation of FDPSO heave motion can be obtained:

$$(m + m_a)\ddot{y} + c\dot{y} + ky = F_v \tag{10}$$

The inherent period of FDPSO is:

$$T = \frac{1}{f} = 2\pi\sqrt{\frac{m + m_a}{k}} \tag{11}$$

In order to reduce the heave performance of FDPSO, the natural period of the platform heave motion can be increased by increasing the additional mass of the structure, so that the natural period of the platform heave motion can be further away from its wave period.

3 Physical model

Based on the actual size of the platform in Table 2, the model was established according to the scale ratio of 1:77.8. The 3D geometric

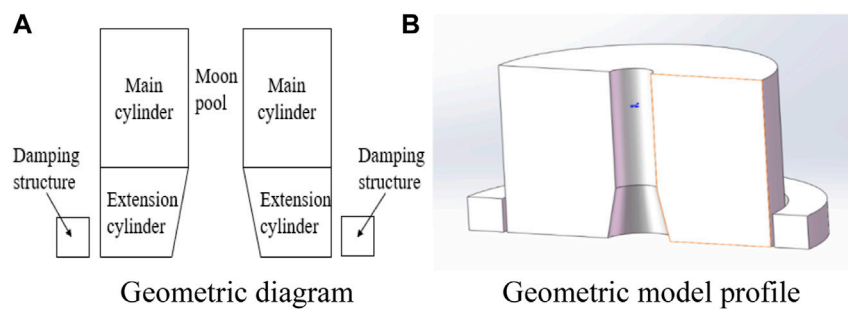


FIGURE 1 Schematic diagram of the geometric model. (A) Geometric diagram. (B) Geometric model profile.

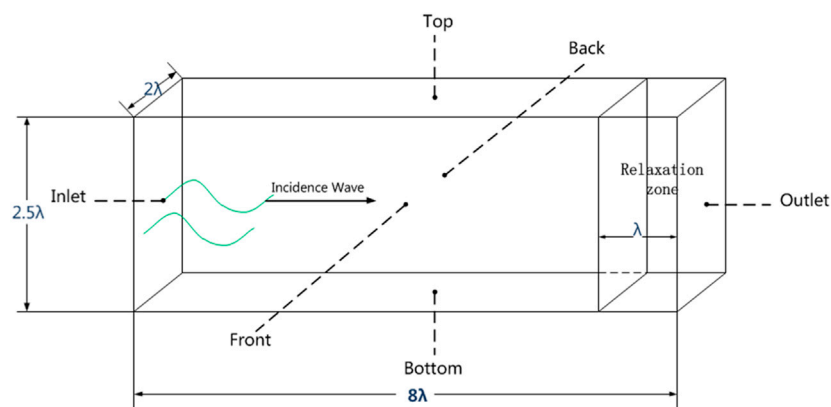


FIGURE 2 Computational domain sketch.

model profile of the platform established based on SolidWorks is shown in Figure 1.

4 Numerical simulation and results discussion

4.1 Computational domain settings and meshing

The model used in this paper is an axisymmetric structure, so half of the model is used for calculation domain setting and grid division. The dimensions of the computational domain are $8\lambda \times 2\lambda \times 2.5\lambda$ (λ is the wavelength), and 8λ , 2λ , and 2.5λ correspond to the length, width, and height of the computational domain respectively. The boundary conditions for Inlet, Back, Bottom, and Top are adopted for velocity inlet, symmetric plane boundary conditions for Front, and pressure Outlet boundary conditions for outlet. In order to prevent the wave reflection phenomenon when the incident wave propagates to the exit, a wave dissipation area is provided at the distance from the exit, and the wave dissipation area adopts damping wave dissipation. The calculation domain sketch is shown in Figure 2. The position of the waterline and the gap between the subtracting structure and the

extended cylinder are encrypted by a three-layer grid, as shown in Figure 3. They are the global grid of the computational domain, the gap out grid and the model surrounding grid.

4.2 Grid convergence verification

In order to conduct convergence analysis on the number of grids, this paper considers the heave attenuation in still water (Bai and Li, 2020), and generates three different numbers of grids when the width and height of the structure with a gap are both 10 m. According to the different number of grids, grid 1, grid 2 and grid 3 are divided, as shown in Table 3.

Three different mesh density models of 1.5 million, 2 million and 2.83 million were used to calculate the heave free attenuation curve, as shown in Figure 4.

Using three different grid density models (1.5 million, 2 million, and 2.83 million cells), the study calculates heave free decay curves for the cylindrical FDPSO with a gap motion reduction structure having widths and heights of 10 m, as depicted in Figure 4. The results obtained using 2 million grid cells closely match those obtained using 2.83 million grid cells, while the results from 1.5 million grid cells show slight discrepancies. Considering computational efficiency, subsequent calculations will use the 2 million grid cells.

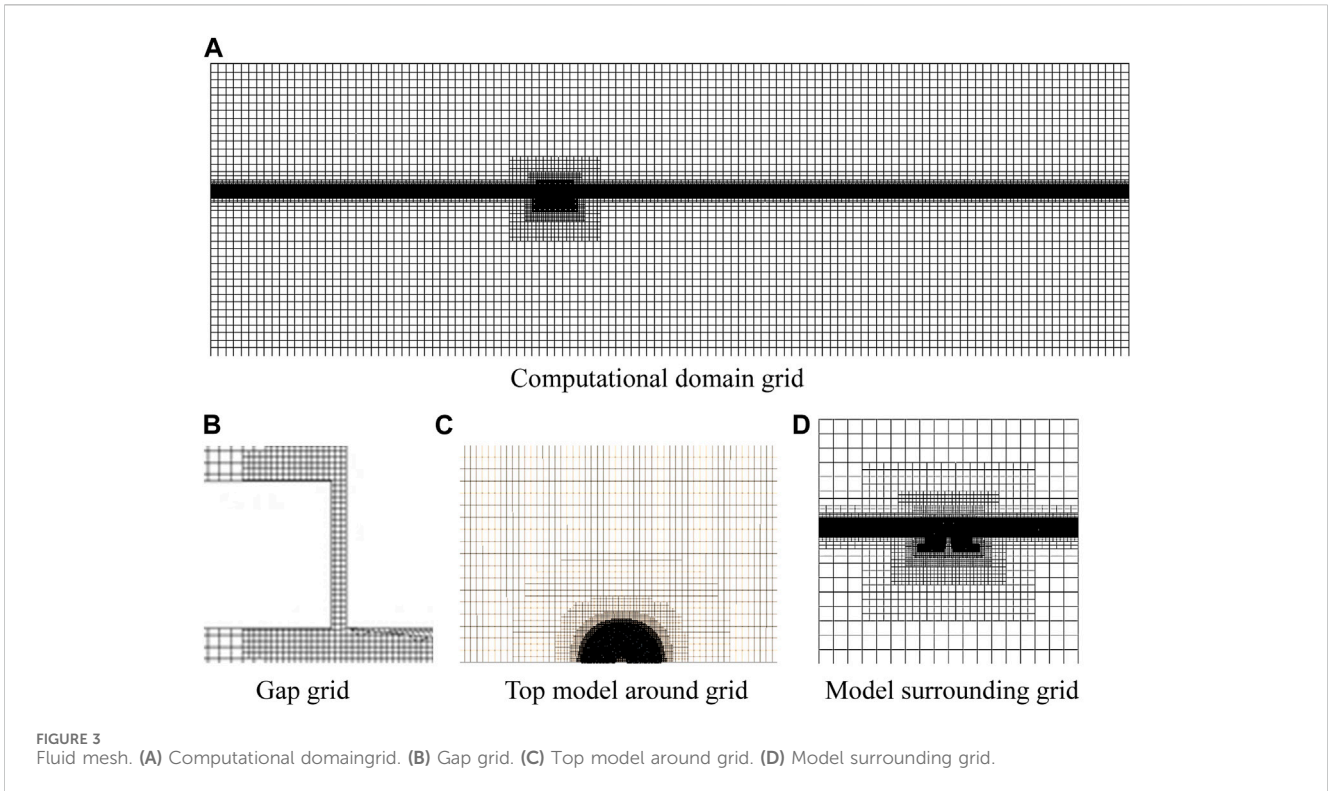
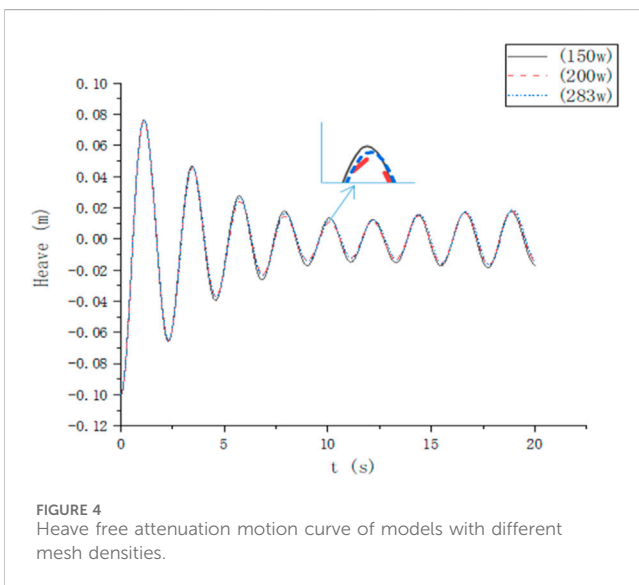


TABLE 3 Mesh convergence verification numerical value of cylindrical FDPSO example.

Grid	Base mesh size/m	Number of grids
Grid1	0.35	1.50×10 ⁶
Grid2	0.3	2.00×10 ⁶
Grid3	0.26	2.83×10 ⁶

4.3 Result analysis

The cylindrical FDPSO used in this study has extended cylindrical bodies and a motion reduction structure. Analyzing the sensitivity of heave motion suppression in the cylindrical FDPSO with varying dimensions of the motion reduction structure, the study investigates different scenarios for the width (10–15 m) and height (10–15 m) of the motion reduction structure, while keeping the other dimension fixed at 10 m. Simulation results for heave motion under different scenarios are presented, and the effect of the motion reduction structure dimensions on the FDPSO’s heave motion is analyzed. The study explores multiple numerical cases considering various widths and heights of the motion reduction structure, presenting the displacement values for different scenarios in [Table 4](#).



4.3.1 Effect of reduced structure width on model heave motion

The heave time history curves for models with widths of 10, 12, and 15 m are simulated and presented in [Figure 5](#). Performing a fast Fourier transform on selected data points, the amplitude-frequency curves shown in [Figure 5](#) demonstrate that increasing the width of the motion reduction structure leads to a gradual reduction in the floater’s amplitude.

Statistical analysis of the heave time history curves for different widths yields the inherent periods of heave motion for models with varying motion reduction structure widths, as shown in [Table 5](#). The data indicates that increasing the width of the motion reduction

TABLE 4 Drainage weight of each size model of anti-motion structure.

Width/m	Actual drained weight/kg	Scale drainage weight/kg	Height/m	Actual drained weight/kg	Scale drainage weight/kg
10	2.034×10^8	431.9	10	2.034×10^8	431.9
11	2.065×10^8	438.5	11	2.062×10^8	437.8
12	2.096×10^8	445.2	12	2.089×10^8	443.7
13	2.129×10^8	452.0	13	2.117×10^8	449.6
14	2.161×10^8	459.0	14	2.145×10^8	455.4
15	2.195×10^8	466.1	15	2.172×10^8	461.2

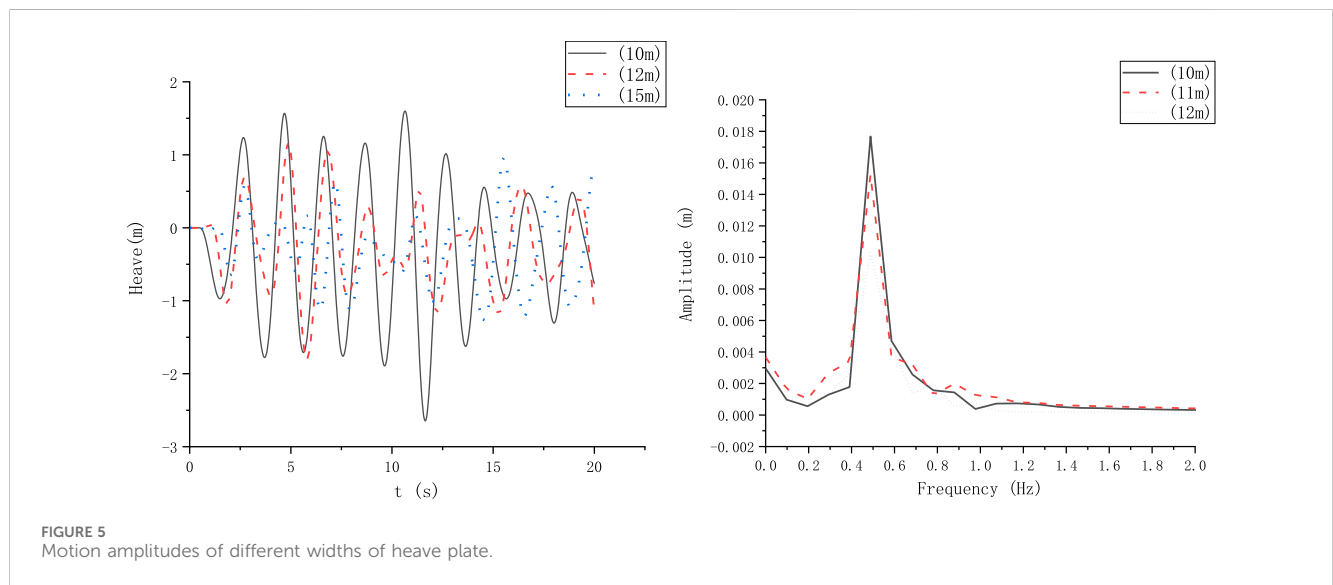


FIGURE 5 Motion amplitudes of different widths of heave plate.

TABLE 5 Heave natural period of different anti-motion structure width.

Reduced structure width/m	Heave natural period/s	Natural period increased by percentage/%
10	2.03	0
11	2.13	4.93
12	2.28	12.32
13	2.42	19.21

TABLE 6 Comparison of heave motion between 10 m and 15 m width.

Movement pattern		The reduced structure is 10 m wide	The width of the reduced structure is 15 m	Difference/%
Heave/m	Max	1.599	0.955	-47.7
	Min	-2.645	-1.266	

structure results in a larger inherent period of heave motion for the cylindrical FDPSO. Compared to the model with a motion reduction structure width of 10 m, models with wider structures exhibit increased inherent periods of 4.93%, 12.32%, and 19.21% for widths of 11, 12, and 13 m, respectively.

Table 6 compares the maximum and minimum values of heave motion for motion reduction structure widths of 10 m and

15 m. The results show that, when considering only floater heave motion, increasing the motion reduction structure width from 10 m to 15 m leads to a decrease in the amplitude of vertical forces, reducing the heave motion of the platform. The heave motion for the platform with a motion reduction structure width of 15 m is reduced by 47.7% compared to the structure with a width of 10 m.

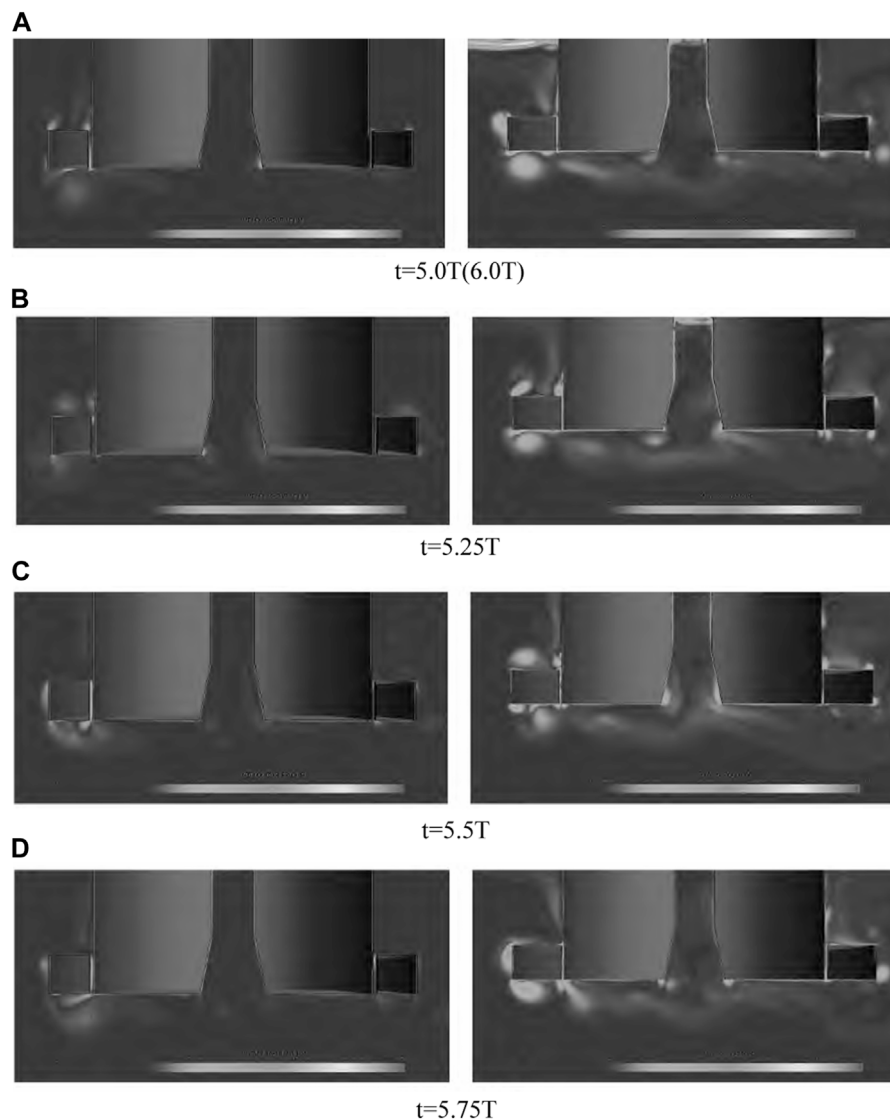


FIGURE 6
The vortex field distribution of different anti-motion structure width. (A) $t=5.0T$ ($6.0T$). (B) $t=5.25T$. (C) $t=5.5T$. (D) $t=5.75T$.

The floating body heave motion is numerically simulated by CFD method. The vorticity of the model with the same height (10 m) and width of 11 m and 14 m in the fifth motion cycle is shown in Figure 6. As can be seen from Figure 6, during the floating body's movement, vortices are generated at the sharp edges and gaps of the reducing structure and the extended cylinder. When FDPSO moves downward from the equilibrium position to the lowest position (5–5.25T), vortices in an upward direction are generated at the top sharp corner of the reducing structure, vortices generated at the bottom sharp corner of the reducing structure form accumulation at the bottom of the floating body, and vortices at the gap move upward. When FDPSO moves upward from the lowest position to the equilibrium position (5.25–5.5T), during the upward movement, the vortices gradually start to fall off, and the vortices falling off at the sharp corners above the reducing structure gradually pile up above the reducing structure, and the vortices falling off at the sharp corners below the reducing structure move backward, and new vortices will be generated at the sharp corners and gaps of the reducing structure.

When FDPSO moves upward from the equilibrium position to a higher position (5.5–5.75T), a downward vortex is generated at the outer sharp corner of the reduced structure. When FDPSO moves downward from the highest position to the equilibrium position (5.75–6.0T), an upward vortex is generated at the sharp corner of the reducing structure, and the vortex gradually falls off with the increase of time. The vortex shed in the early stage continues to move away from the cylindrical FDPSO and gradually dissipates in the surrounding flow field. On the whole, the vortex structure generated by sharp edges and gaps in the process of motion presents a tendency of dissipation and propagation to the surrounding flow field (Bai and Li, 2020). The vorticity generation and dissipation of models with large widths are increased compared with those with small widths.

In summary, the increase of the width of the cylindrical FDPSO damping structure increases the natural period of the heave motion of the structure, making it far away from the range of the main energy period of the wave, and can effectively slow down the heave motion of the platform.

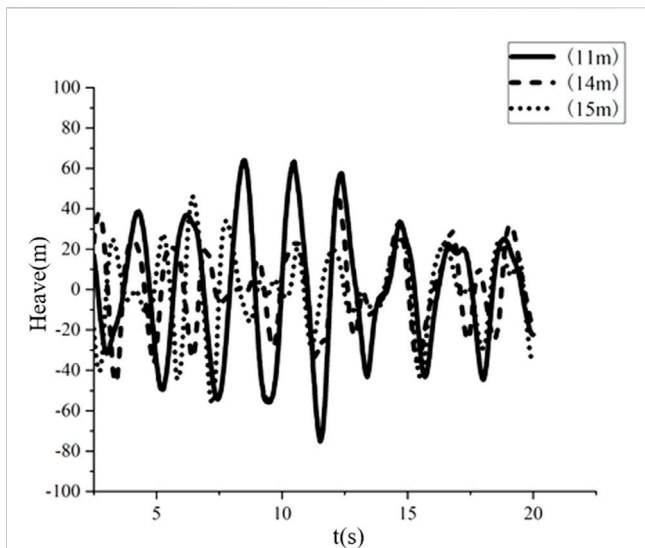


FIGURE 7 Vertical stress time curve of different decreasing structure widths.

4.3.2 Effect of reduced structure height on model heave motion

Through numerical simulation of the heave motion of the model with a height of 10, 11, 12, 13, 14 and 15 m of the reduced structure, the heave time curve is obtained. Figure 8 shows the heave time curve of the model with a height of 13 and 15 m. Take some data for fast Fourier transform and draw the amplitude-frequency curve as shown in Figure 8. As can be seen from Figure 8, the height of the subtractive structure increases, while the floating body amplitude gradually decreases.

According to the statistics of the heave time curve of the different height of the subtraction structure, the natural heave period of the model with different height of the subtraction structure can be obtained, as shown in Table 7. The natural period of the real scale platform movement is obtained by scaling ratio conversion. When the height of the subtraction structure is

10 m, its heave natural period is 17.91 s. When the height is 13 m, the natural period is 18.52 s. When the height is 15 m, the natural period is 19.23 s. The data in Table 7 show that the natural period of heave motion of cylindrical FDPSO increases with the increase of the height of the subtraction structure. Compared with the model with a height of 10 m, the natural period of other height models increases by 3.45% and 7.93%, respectively.

Table 8 compares the maximum and minimum values of heave motion of a subtractive structure with a height of 13 m and a height of 15 m. It can be seen that when only the heave motion of the floating body is considered, when the height of the decreasing structure increases from 13 m to 15 m, the amplitude of the vertical force of the floating body decreases, which reduces the heave motion of the platform. The heave motion of the platform with the height of the decreasing structure is 43.1% lower than that of the platform with the height of the decreasing structure is 13 m.

The vorticity diagram of the model with constant width (10 m) and height of 12 m and 15 m in the sixth motion cycle is shown in Figure 9. It can be seen that vortices are generated in the sharp edges and gaps of the reducing structure and the extended cylinder during the floating body's movement. When FDPSO moves downward from the equilibrium position to the lowest position (6–6.25T), vortices in the upward direction are generated at the top sharp corner of the reducing structure, vortices generated at the bottom sharp corner of the reducing structure form accumulation at the bottom of the floating body, and vortices at the gap move upward. When FDPSO moves upward from the lowest position to the equilibrium position (6.25–6.5T), the vortices gradually start to fall off during the upward movement, and the vortices falling off at the sharp corners above the reducing structure gradually pile up above the reducing structure, and the vortices falling off at the sharp corners below the reducing structure move backward, and new vortices will be generated at the sharp corners and gaps of the reducing structure. When FDPSO moves upward from the equilibrium position to a higher position (6.5–6.75T), a downward vortex is generated at the outer sharp corner of the structure. When the FDPSO moves downward from the highest position to the equilibrium position (6.75–7.0T), an upward vortex is generated at the sharp corner of the reducing structure, and the

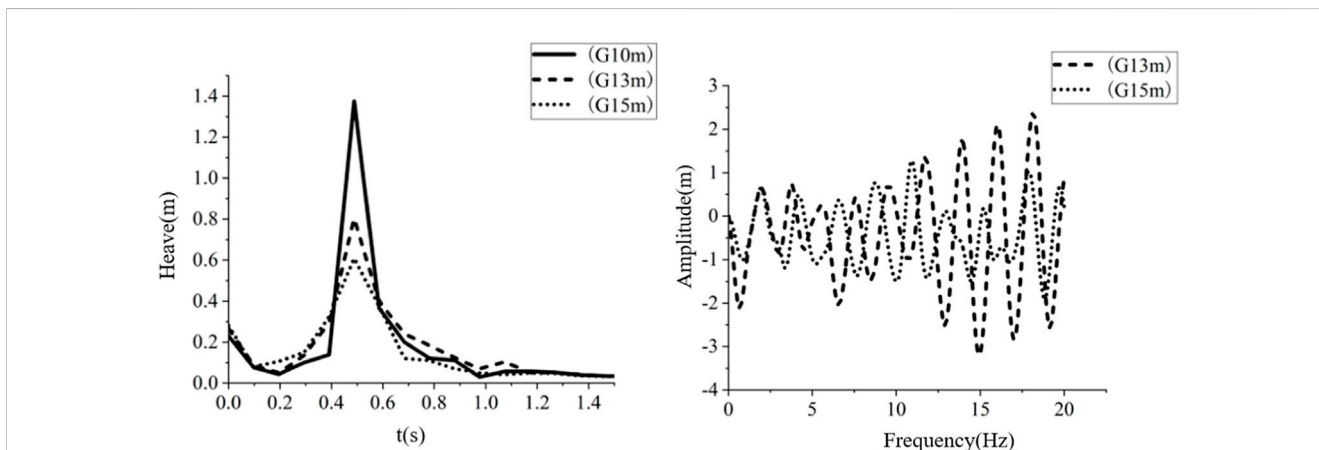


FIGURE 8 Motion amplitudes of different widths of heave plate.

TABLE 7 Sag natural period of different height of subtraction structure.

Reduced structural height(m)	Proper period(s)	Natural period increased by percentage
10	2.03	0
13	2.10	3.45%
15	2.18	7.39%

TABLE 8 Comparison of heave motion between 13 m and 15 m heights.

Movement pattern		The reduced structure is 13 m wide	The width of the reduced structure is 15 m	Difference/%
Heave/m	Max	2.376	1.281	-43.1
	Min	-3.206	-1.894	

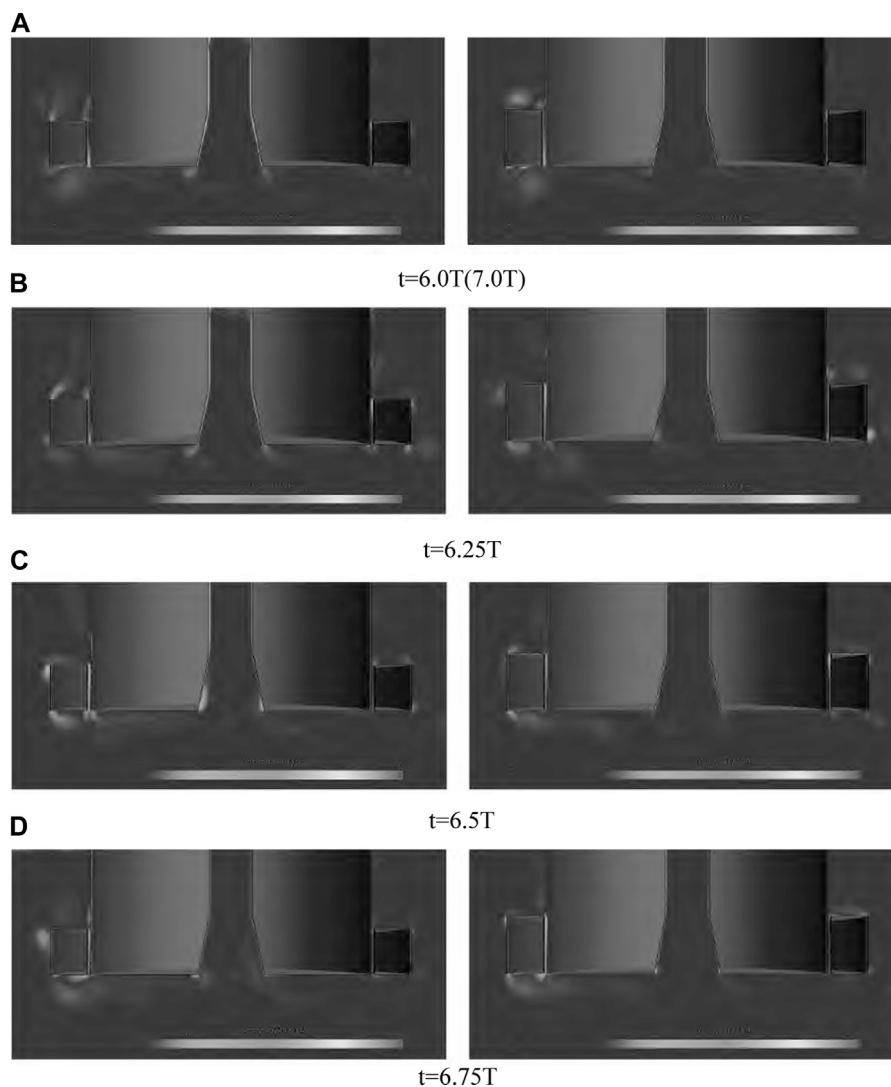
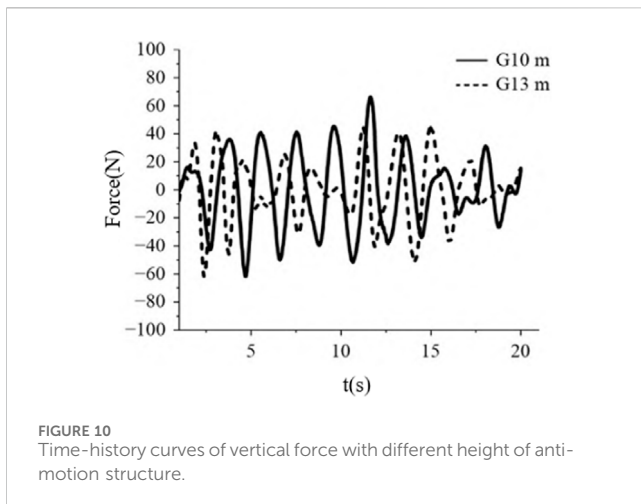


FIGURE 9 The vortex field distribution of different anti-motion structure height. (A) $t=6.0T$ (7.0T). (B) $t = 6.25T$. (C) $t = 6.5T$. (D) $t = 6.75T$.

vortex gradually falls off with the increase of time. The vortex shed in the early stage continues to move away from the cylindrical FDPSO and gradually dissipates in the surrounding flow field. On the whole,

the vortex structure generated by edge sharp corners and gaps in the process of motion shows a tendency to dissipate and propagate to the surrounding flow field. The vorticity generation and dissipation



increase with the increase of height, but the vorticity change is not obvious compared with that with the increase of width.

Figure 10 shows the time history curve of the vertical force of the model with different height of the subtraction structure. In this paper, the effect of fluid viscosity is considered in the research process. The viscosity of liquid will produce resistance to objects in motion, that is, the viscous pressure resistance. Relative movement will cause the pressure difference between the front and back of the reduced structure. The vertical stress amplitude of the floating production unit is reduced, but the change of the height of the damping structure has little effect on the viscous pressure difference.

In summary, the natural period of heave motion can be increased with the increase of height of cylindrical FDPSO, but the increase of natural period caused by the increase of height is smaller than that caused by the increase of width.

5 Conclusion

In this paper, STAR-CCM+, a computational fluid dynamics software, is used to numerically simulate the heave motion of a new cylindrical FDPSO with different widths and heights under the action of irregular waves. According to the calculation results, the following conclusions are drawn:

- (1) under the condition of fixed height of the subtraction structure, increasing the width of the subtraction structure can effectively increase the natural period of the heave motion of the new cylindrical FDPSO, making it far away from the cycle range of the main energy of the wave, that is, increasing the width can inhibit the heave motion of the floating production unit.
- (2) Under the condition that the width of the reduced structure is fixed, the increase of the height of the reduced structure also increases the natural period of the heave motion of the new cylinder type FDPSO to a certain extent, which has an inhibiting effect on its heave motion.
- (3) During the movement of the new cylinder type FDPSO, vortices are generated at the sharp edges of the extended cylinder and the reducing structure, especially at the gap between the reducing structure and the extended cylinder.

- (4) The generation and shedding of vortices around the high-width subtraction structure model is significantly increased compared with that of the low-width subtraction structure model, resulting in an increase in the friction resistance of the subtraction structure; Compared with the width change, the generation and shedding of the vortex caused by the change of height is relatively weak, and the increase of height leads to the increase of friction resistance of the structure.
- (5) The increase of the size of the subtraction structure can inhibit its sag motion. And compared to the height increasing the suppression effect on floating platform, increasing the width of the platform more obvious suppression effect.

Data availability statement

The original contributions presented in the study are included in the article/Supplementary material, further inquiries can be directed to the corresponding author.

Author contributions

HY: Conceptualization, Data curation, Formal Analysis, Methodology, Validation, Visualization, Writing—original draft. YC: Formal Analysis, Investigation, Software, Validation, Visualization, Writing—original draft. ML: Investigation, Methodology, Project administration, Resources, Writing—review and editing. LC: Formal Analysis, Validation, Visualization, Writing—review and editing. XB: Investigation, Project administration, Writing—review and editing. YL: Investigation, Project administration, Writing—review and editing.

Funding

The author(s) declare that financial support was received for the research, authorship, and/or publication of this article. National Natural Science Foundation of China, Surface Project, 42276225, Research on magnetic-electric-fluid-Solid multi-field and multiphase Coupling Characteristics and Power generation Efficiency of improved magnetic levitation VIVACE Tidal current power generation Device, 2023-01-01 to 2026-12-31, 540,000 yuan, in research, participate Science and Technology Department of Jiangsu Province, Natural Science Foundation of Jiangsu Province (Surface Research Project), BK20211342, Study on fluid-induced vibration Mechanism and Energy capture Characteristics of multi-cylindrical oscillators supported by magnetic levitation, 2021-07 to 2024-07, 100,000 yuan, participated.

Conflict of interest

Author HY was employed by Shanghai Waigaoqiao Shipbuilding and Ocean Engineering Co., LTD.

The remaining authors declare that the research was conducted in the absence of any commercial or financial relationships that could be construed as a potential conflict of interest.

Publisher's note

All claims expressed in this article are solely those of the authors and do not necessarily represent those of their affiliated

organizations, or those of the publisher, the editors and the reviewers. Any product that may be evaluated in this article, or claim that may be made by its manufacturer, is not guaranteed or endorsed by the publisher.

References

- Bai, J., and Li, Y. (2020). Optimization design of heave suppression structure for new cylindrical FPSO. *J. OCEAN Eng.* 38 (1), 20–29.
- Du, Y. H. (2021). Numerical analysis of ship motion response characteristics in irregular waves. *J. THE Ocean. Eng.* 39 (3), 31–41.
- Gorma, W., Post, M. A., White, J., Gardner, J., Luo, Y., Kim, J., et al. (2021). Development of modular bio-inspired autonomous underwater vehicle for close subsea asset inspection. *Appl. Sci.* 11 (12), 5401. doi:10.3390/app11125401
- Guo, L. (2017). *Numerical simulation of tank sloshing based on VOF method*. Harbin, China: D. Harbin Engineering University.
- Hirt, C. W., and Nichols, B. D. (1981). Volume of fluid (VOF) method for the dynamics of free boundaries. *J. Comput. Phys.* 39 (1), 201–225. doi:10.1016/0021-9991(81)90145-5
- Ji, R., Sun, K., Zhang, J., Zhu, R., and Wang, S. (2022). A novel actuator line-immersed boundary (AL-IB) hybrid approach for wake characteristics prediction of a horizontal-axis wind turbine[J]. *Energy Conversion and Management* 253, 115193.
- Li, M., Yuan, Z.-M., Bai, X., Li, Y. Z., Cheng, Y., and Tao, L. (2023a). Numerical modelling of wash waves generated by ships moving over an uneven bottom. *China Ocean Engineering* 37 (1), 145–153.
- Li, M., Yuan, Z.-M., and Tao, L. (2023b). Wash waves generated by ship moving across a depth change. *Ocean Engineering* 275, 114073.
- Li, M., Chen, Y., Yuan, Z.-M., Cheng, Y., and Tao, L. (2023c). Interference effects on the upstream wave generated by the catamaran moving across a depth change. *Ocean Engineering* 287, 115939.
- Li, M., Pan, S., Cheng, Y., Yuan, Z.-M., and Tao, L. (2023d). Time-domain numerical simulation for multi-ships moving in waves with forward speed. *Ocean Engineering* 290, 116325.
- Li, M., Yuan, Z.-M., Ji, C., Li, L., Jia, L., and Atilla, I. (2019). Steady hydrodynamic interaction between human swimmers. *Journal of Royal Society:Interface* 16, 1–12.
- Liu, L. Q., and Zhang, X. R. (2019). Damping characteristics of cone damping structure on FDPSO based on CFD. *J. CHINA OFFSHORE Platf.* 34 (3), 25–31.
- Wang, S. S., and Zhao, J. R. (2014). Global performance analysis for deep water octagon FDPSO. *J. S. HI P OCE Eng.* 43 (3), 183–186+189.
- Wang, T. Y., and Feng, Y. X. (2011). Advanced development of research on new concept FPSOs. *J. S. HI P OCE Eng.* 40 (5), 184–188+192.
- Yao, Y. X., and Wang, W. H. (2015). Analysis on heave motion performance of new sandglass-type floating body. *J. Huazhong Univ. Sci. & Tech. Natural Sci. Ed.* 43 (7), 129–132.
- Zeng, X., Shao, Y., Feng, X., Xu, K., Jin, R., and Li, H. (2024). Nonlinear hydrodynamics of floating offshore wind turbines: A review[J]. *Renewable and Sustainable Energy Reviews* 191, 114092.
- Zeng, X., Shi, W., Feng, X., Shao, Y., and Li, X. (2023). Investigation of higher-harmonic wave loads and low-frequency resonance response of floating offshore wind turbine under extreme wave groups[J]. *Marine Structures* 89, 103401.
- Zeng, X., Shi, W., Michailides, C., Zhang, S., and Li, X. (2021). Numerical and experimental investigation of breaking wave forces on a monopile-type offshore wind turbine[J]. *Renewable Energy* 175, 501–519.
- Zhao, Z. J. (2012). *Concept design and research on the hydrodynamic performance of a multi-cylindrical FDPSO*. Tianjin: D. Tianjin University.